https://doi.org/10.2352/ISSN.2470-1173.2021.6.IRIACV-335

Object Alignment with Refocused Image Using Off-Axis Digital Holography

Fan Hei Hung; Department of Electrical and Electronic Engineering, The University of Hong Kong; HKSAR, China
Edmund Y. Lam; Department of Electrical and Electronic Engineering, The University of Hong Kong; HKSAR, China

Abstract

In the semiconductor industry, the integrated circuit density is getting higher, which leads to a smaller margin of error for the bonding process. Therefore, accurate adjustments before bonding are often necessary. An accurate image alignment under a vision system is usually required to fine-tune the bonding position. However, a considerable depth of focus is sacrificed for sufficient resolution of the object, limiting the optics operation range. Digital holographic microscopy with digital refocusing is applied as an enhancement to extend the depth of focus. The proposed algorithm merges the image alignment method with a refocusing algorithm to extend the image alignment capability with digital holography. Tested with simulated images, the proposed algorithm showed no significant deviation to simulated parameters. Also, the alignment result is robust among several test patterns. Moreover, the overall time is reasonable for industrial application.

Introduction

Since 1960s, there is an observation in the semiconductor industry that the number of transistors on a chip doubles every two years, named Moore's Law. As the integrated circuit density is getting higher, the transistor size also decreases, currently as small as a few nanometers. To ensure a high-quality bonding process, a vision system has been adopted as a standard solution to evaluate the offsets through image alignment, and the offsets are corrected with an actuator. However, the depth of focus is shorter for a higher resolution. The optics operation range is limited as the depth of focus is fixed after selecting enough resolution for viewing the object. To achieve larger depth of focus of the image, digital holographic microscopy using digital refocusing is applied to extend the depth of focus. The digital refocusing result can also provide extra 3D information, such as tilting, as new alignment features.

Digital Holographic Microscopy (DHM)

A hologram is a recording of the light interference pattern. The information captured in the hologram includes the 3D information of any objects within the light path. 3D measurements are possible from the recovered information. The science of using hologram is called holography, invented by Denis Gabor in 1947 [1]. Among the sub-branches of holography, DHM, as the topic of interest, shares the same principle as conventional holography but uses a digital sensor to capture the hologram and a microscope objective to enlarge the object. With enlarging capability, DHM application is most commonly found in biomedical [2] and engineering fields [3].

Off-Axis DHM

Typical holography configuration involves using a coherent laser light source, split into an object beam O and reference beam R. Under a reflection configuration, the object beam illuminates the target object. It gets back to the hologram H by reflection on the surface. Then according to the superposition principle, the hologram interference intensity is

$$H = |O+R|^2 = |O|^2 + |R|^2 + O^*R + OR^*, \tag{1}$$

where O^* and R^* are the complex conjugate of O, and R respectively.

Off-axis holography configuration, invented by Emmett Leith and Juris Upatnieks [4], is one of the methods to recover the object beam information from a single hologram. Off-axis configuration introduces a small angle difference between the object and the reference beam. The tilted reference beam R_{off} introduces a tilted phase term relative to the object plane, such that

$$R_{\text{off}}(x,y) = e^{i2\pi(x\widehat{f_x}+y\widehat{f_y})}R(x,y), \tag{2}$$

where x, y are the coordinates in the spatial domain, and $\widehat{f_x}$, $\widehat{f_y}$ are the slope caused by the tilting. The tilting of the cross term is determined by

$$\widehat{f_x} = \frac{\lambda}{\sin\phi_x}, \widehat{f_y} = \frac{\lambda}{\sin\phi_y}, \tag{3}$$

where ϕ_x, ϕ_y is the tilting angle in x, y direction and λ is the laser light wavelength. Using the frequency shifting properties causes the cross term OR^* and O^*R to shift in the hologram angular spectrum. The tilted reference beam in angular spectrum becomes

$$\widehat{R_{\text{off}}}\left(f_x, f_y\right) = \widehat{R}\left(f_x - \hat{f}_x, f_y - \hat{f}_y\right), \tag{4}$$

where f_x, f_y are the coordinates in the angular spectrum, $\widehat{R}$ and $\widehat{R_{\text{off}}}$ are the Fourier transform of R and R_{off} respectively. A box filter with a known tilting $\widehat{f_x}$, $\widehat{f_y}$ and a selected bandwidth W_x,W_y is often used to isolate the OR^* term by

$$\widehat{OR^*} \approx \text{rect}\left(\frac{f_x+\widehat{f_x}}{W_x}\right)\text{rect}\left(\frac{f_y+\widehat{f_y}}{W_y}\right)\widehat{H}(f_x,f_y), \tag{5}$$

which the bandwidth is often chosen to capture most of the information. After that, the extracted term divides with R^* to get O.

Extended Depth of Field (DoF) with Digital Refocusing

One of the benefits of DHM is its ability to extend DoF by digital refocusing. With the extracted complex wave-front from a hologram, the wave-front at specific heights can be simulated through Fourier optics [5]. The method used in this paper is called the angular spectrum (AS), which involves three main steps. The first step is to take the wave-front to angular spectrum by Fourier transform (FT). The second step is to multiply a phase change propagation term,

$$\widehat{O}(f_x,f_y;z) = e^{iz\frac{2\pi}{\lambda}\sqrt{1-(\lambda f_x)^2-(\lambda f_y)^2}}\widehat{O}(f_x,f_y;0). \quad (6)$$

Finally, the altered spectrum is brought back to the spatial domain through inverse FT.

Object Alignment with Hologram

While typical object alignment can search for an object within a 2D plane, alignment with hologram can search within a 3D region. There have been a few attempts for object alignment using complex wave-front. Kim et al. proposed to use Wigner distribution functions to estimate the translation in the 3D space [6]. Seifi et al. proposed a method of object recognition by diffraction-pattern matching [7]. Abeywickrema et al. used correlation of hologram to estimate the translation of fingerprint [8]. Most of the approaches did not require to align a tilted planar object, which is a useful feature in bonding applications. This paper attempts to use a hologram alignment model with 3D translation and a planar object's tilting.

The alignment process first requires a template hologram H_T, captured from a reference orientation. Then, the target hologram H_I is captured for each alignment case relative to the same template hologram. As the reference beam does not change among the template and target hologram, the reference tilting angle ϕ_x, ϕ_y, the central frequency $\hat{f}_x$, $\hat{f}_y$ and bandwidth W_x, W_y becomes a constant. The five independent variables for alignment are then defined as follows: $\hat{x}$, $\hat{y}$, $\hat{z}$ corresponds to the relative translation in x, y, z direction respectively; $\hat{\theta}_x$, $\hat{\theta}_y$ corresponds to the relative tilting along x, y axis respectively.

While image translation $\hat{x}$, $\hat{y}$ on the x,y plane is self-explanatory, the relation between holograms of height translation $\hat{z}$ and tilting $\hat{\theta}_x$, $\hat{\theta}_y$ of the object is described as below.

For simplicity, O_T and O_I are used to represent the template and the target object, respectively. The relation between object, hologram and reference can refer to equation 1. The height translation $\hat{z}$ of the object can use the angular spectrum method and numerically propagate the template image, as specified in equation 6. Tilting of the object wave-front $\hat{\theta}_x$, $\hat{\theta}_y$ can be expressed as an additional tilting phase on the template phase using thin element approximation

$$O_I(x,y) \approx \exp\left[-\frac{i2\pi}{\lambda}2\left(x\tan\hat{\theta}_x + y\tan\hat{\theta}_y\right)\right] O_T(x,y). \quad (7)$$

A multi-step approach is proposed to solve the $\hat{x}$, $\hat{y}$, $\hat{z}$ translation, and $\hat{\theta}_x$, $\hat{\theta}_y$ tilting.

Proposed Algorithm

The proposed algorithm's key is to bring both the template hologram and the target hologram to the angular spectrum. After that, the template object information O_T and target object information O_I is extracted using equation 5. Then, use a 2D image alignment method to find the translation of the spectrum amplitude. The translation corresponds to the object tilting, as a reference to equation 7, tilting in phase causes a translation in spectrum amplitude, such that

$$\widehat{O_I}(f_x,f_y) \approx \widehat{O_T}\left(f_x + \frac{2\tan\hat{\theta}_x}{\lambda}, f_y + \frac{2\tan\hat{\theta}_y}{\lambda}\right). \quad (8)$$

In this paper, the enhanced correlation coefficient (ECC) maximization algorithm is used for 2D alignment of the spectrum amplitude [9]. ECC algorithm first computes a zero mean, normalized image of the template and initializes a translation guess. The target image is then translated and normalized to compute the correlation with the template and update the translation until convergence. The result can transform into tilting θ_x, θ_y using equation 8.

After the spectrum amplitude is aligned, obtain the phase difference Φ by

$$\Phi(f_x,f_y) = \arg\left(\widehat{O_I}\right) - \arg\left(\widehat{O_T}\right), \quad (9)$$

where for a generic complex z, $\arg(z)$ is the phase of z.

From the angular spectrum method in equation 6, and also the spatial shift properties of Fourier transform, the phase difference is related to the $\hat{x}$, $\hat{y}$, $\hat{z}$ translation by

$$\Phi(f_x,f_y) = -2\pi\left(\hat{x}f_x + \hat{y}f_y - \hat{z}\sqrt{\frac{1}{\lambda^2} - f_x^2 - f_y^2}\right). \quad (10)$$

To provide a reasonable estimate of the $\hat{x}$, $\hat{y}$, $\hat{z}$ translation from the wrapped phase data, fitting of the phase is required. In 2015, X. Tong proposed an approach for getting shift from 2D alignment and tested it with real satellite images [10]. Instead of using the traditional phase correlation approach, the paper takes the phase data to fit the slope tilting. The slope of the fitted phase can transform into a shift in the spatial domain. As a reference, this paper attempts to use a similar approach to fit the curved phase.

First, to avoid the 2π phase jump in the phase angle, the first derivative in phase is used for fitting instead of the absolute phase. For simplification, the angular spectrum relation is approximated with Taylor expansion to give

$$\Phi(f_x,f_y) \approx -2\pi\left[\hat{x}f_x + \hat{y}f_y - \hat{z}\left(\frac{1}{\lambda^2} - \frac{f_x^2}{2} - \frac{f_y^2}{2}\right)\right]. \quad (11)$$

Then, derivative in the x and y direction becomes

$$\left[\frac{\partial\phi(f_x,f_y)}{\partial f_x}\right]_{2\pi} = -2\pi\left(\hat{x} + \hat{z}f_x\right), \quad (12)$$

$$\left[\frac{\partial\phi(f_x,f_y)}{\partial f_y}\right]_{2\pi} = -2\pi\left(\hat{y} + \hat{z}f_y\right), \quad (13)$$

where for a generic real x, $[x]_{2\pi} = x + 2\pi n$, with n the integer that $[x]_{2\pi} \in [-\pi,\pi)$.

After that, a robust fitting algorithm, proposed by Paul. W. Holland and Roy E. Welsch [11], is used to fit the phase derivative as tilting plane. This algorithm refines the regression result by

re-weighting the contribution of each sample points until convergence. Therefore, choosing suitable initial weighting can create a quick convergence. For this case, the logarithm of the spectrum amplitude is suitable. For low spectrum amplitude, image noise often dominates, and the phase is unreliable. Also, taking the spectrum amplitude logarithm prevents the wide range of the weighting that regression may compute near matrix singularity. A further improvement to remove outlier is to set a threshold on the spectrum amplitude such that image noise contribution is filtered out. Assuming a Gaussian distribution of image noise, the threshold η is set to

$$\eta = \sqrt{-var(\partial\Phi)\log_e \alpha}, \tag{14}$$

where α is the tail probability of finding the image noise from the spectrum amplitude, $\log_e$ is the natural logarithm notation, and $var(x)$ is the variance of the image noise.

Finally, the fitting result will be transformed into $\hat{x}$, $\hat{y}$, $\hat{z}$ translation using equation 12, 13.

Method

To evaluate the proposed algorithm, a template hologram and three target holograms from 3 patterns (circle, triangle and cross) are generated through simulation. All target holograms are then passed to the algorithm to compute the shifts and tilting relative to the template hologram. Then, the results are analysed for effectiveness, robustness and timing.

The first simulated image dataset is a synthetic circle pattern hologram template and three target holograms with different shifts or tilting. It aims to evaluate the effectiveness and robustness of handling noise originating from the digital sensor. The second and third image datasets are a synthetic triangle and cross template, respectively. Each set has three target holograms with different shifts or tilting. All the three image datasets aim to evaluate the robustness of handling different alignment patterns. Moreover, all datasets provide an average overall run-time as a reference.

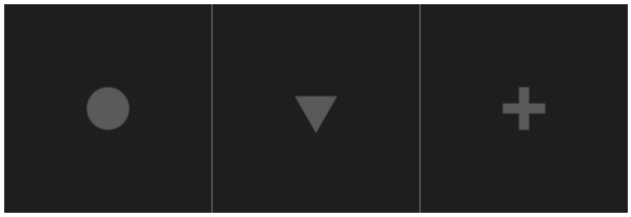

Figure 1. *Template holograms from left to right: circle pattern, triangle pattern and cross pattern*

All synthetic image datasets were generated from the template pattern as shown in figure 1. First, to simulate the pattern as a grabbed image, the following parameter are used: laser wavelength $\lambda = 0.633\mu m$, image resolution = $0.345\mu m$, image size = 1024×1024, $\hat{f}_x = 0.98\mu m^{-1}$, $\hat{f}_y = 1.16\mu m^{-1}$, $W_x = W_y = NA = 0.23$. All images are Gaussian smoothed according to the image NA (0.23) before interference with reference beam. The image is cast to an 8-bit image added with Gaussian noise of 1 standard deviation gray-level. Each pattern is used to generate 1 template hologram and 3 alignment hologram with following shift and tilting, refering to table 1.

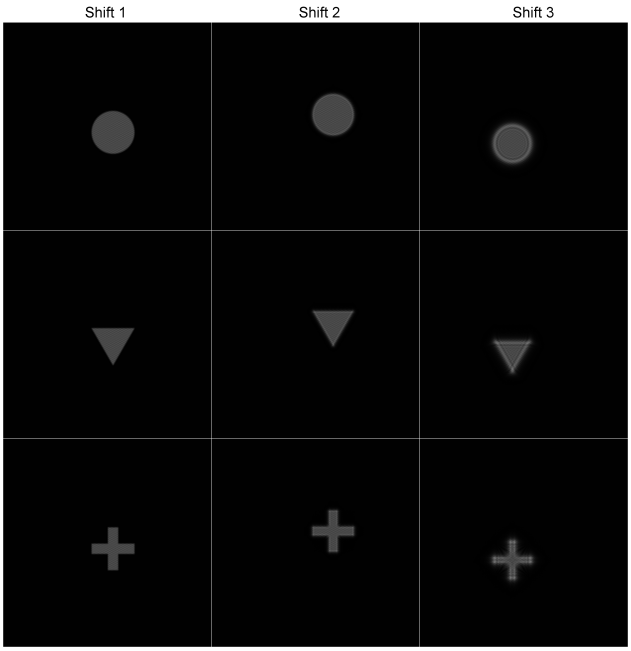

Figure 2. *Sample images for alignment: from left to right are the three simulated shift and tilting in order, as specified in table 1. Each image row corresponds to one pattern (circle, triangle, cross).*

Table 1: Simulation for different shifts and tiltings for each template pattern

	$\hat{x}(\mu m)$	$\hat{y}(\mu m)$	$\hat{z}(\mu m)$	$\hat{\theta}_x(rad)$	$\hat{\theta}_y(rad)$
Shift 1	10	10	0	0	0
Shift 2	30	-20	30	0	0
Shift 3	-20	30	-100	0.2	-0.3

From the table, the first target only involves the planar translation of the template. The second target hologram has additional plane propagation, and the third target hologram includes extra tilting. Figure 2 shows the target holograms corresponding to target 1,2 and 3 for the three types of the pattern used in the dataset.

The estimated accuracy for $\hat{x}$, $\hat{y}$, $\hat{z}$ translation depends on the optics resolution, which is also related to wavelength λ and numeric aperture (NA). The limit computed in equation 15 provides an expected performance for the algorithm.

$$\delta x = \delta y = \frac{0.61\lambda}{NA}, \delta z = \frac{\lambda}{NA^2}, \tag{15}$$

where δx, δy, δz are the maximum error of the translation estimation of $\hat{x}$, $\hat{y}$, $\hat{z}$ respectively. The maximum estimated error $\delta\theta_x$, $\delta\theta_y$, for tilting$\hat{\theta}_x$, $\hat{\theta}_y$, is the frequency resolution in the angular spectrum. In terms of radian, the relation to the maximum error is

$$\delta\theta_x = \delta\theta_y = \tan^{-1}(\lambda/2N)rad. \tag{16}$$

The test code is implemented on a computer with Intel i7 Core, CPU at 2.60GHz, using MATLAB R2019B to test the algorithm's effectiveness, robustness, and timing. Each template's alignment case undergoes 1000 repetitions to measure the average and range of aligned position and time.

Results and Discussion

The alignment results of the three types of patterns are summarized in table 2, 3 and 4. Each table contains three columns, representing the results of the three different shifts and tilting as specified in table 1. Each row of the table represents the five variables that is solved through the algorithm, which is $\hat{x}$, $\hat{y}$, $\hat{z}$ translation, and $\hat{\theta}_x$, $\hat{\theta}_y$ tilting. Each cell of the table contains 1000 averaged results of the estimation with added noise and a range of 3 standard deviations of the result.

Table 2: Alignment error summary for circle pattern

	Shift 1	Shift 2	Shift 3
$\hat{x}(\mu m)$	10.00±0.25	30.05±0.25	-20.25±0.26
$\hat{y}(\mu m)$	10.00±0.24	-19.94±0.26	30.93±0.27
$\hat{z}(\mu m)$	-0.05±5.06	30.90±5.15	-109.64±6.00
$\hat{\theta}_x(rad)$	0.00±0.00007	0.00±0.00007	0.20±0.00007
$\hat{\theta}_y(rad)$	0.00±0.00007	0.00±0.00007	-0.30±0.00006

Table 3: Alignment error summary for triangle pattern

	Shift 1	Shift 2	Shift 3
$\hat{x}(\mu m)$	9.99±0.27	30.04±0.26	-19.83±0.25
$\hat{y}(\mu m)$	10.00±0.27	-19.95±0.28	29.95±0.27
$\hat{z}(\mu m)$	-0.06±4.03	30.22±4.16	-100.50±3.95
$\hat{\theta}_x(rad)$	0.00±0.0001	0.00±0.0001	0.20±0.0001
$\hat{\theta}_y(rad)$	0.00±0.0001	0.00±0.0001	-0.30±0.0001

Table 4: Alignment error summary for cross pattern

	Shift 1	Shift 2	Shift 3
$\hat{x}(\mu m)$	10.03±0.26	30.10±0.26	-20.18±0.28
$\hat{y}(\mu m)$	10.03±0.25	-20.00±0.27	30.57±0.29
$\hat{z}(\mu m)$	-0.05±4.28	30.09±4.26	-103.53±4.85
$\hat{\theta}_x(rad)$	0.00±0.0001	0.00±0.0001	0.20±0.0001
$\hat{\theta}_y(rad)$	0.00±0.0001	0.00±0.0001	-0.30±0.0001

Firstly, by comparing the average result of all variables with the simulated value, the algorithm's effectiveness in handling noise are interpreted. Also, the theoretical resolution limit must bound the deviation of the result. In theory, using equation 15, 16 and the parameters as given in the previous section, the dataset used in the experiment shares the following maximum error: $\delta x = \delta y = 1.67\mu m, \delta z = 11.96\mu m, \delta\theta_x = \delta\theta_y = 0.0003rad$. From table 2, all $\hat{x}$, $\hat{y}$, $\hat{z}$, $\hat{\theta}_x$, and $\hat{\theta}_y$ shows a very close average result to the simulated value for the first two columns. The deviations are smaller than the expected maximum error. However, the average estimation of $\hat{z}$ is slightly larger than the simulated value in the third column, which has a larger propagation distance. It is likely to be caused by the approximation of the propagation term with a quadratic function. As there is the residue after the quadratic approximation, the fitted derivative contains a larger model error, which may fluctuate more than a result with a smaller propagation distance. Nonetheless, the algorithm is effective for small propagation distance.

Secondly, by comparing the results among the 3 pattern images, the algorithm's robustness is evaluated. Similarly from table 3, 4, the averaged result and deviation are close to the simulated value and the expected maximum error. The insignificant difference in result for different pattern shows the robustness of the algorithm.

Finally, using the image dataset, the overall run time of the algorithm is obtained for reference. The total time used has an average of $210ms$. For further investigation, the algorithm's three different steps can break down the overall timing into three parts. The first part is to take the image to an angular spectrum, which requires to compute one Fourier transform, and the actual average time used is $10ms$. The second step is to perform ECC alignment to compute $\hat{\theta}_x$, $\hat{\theta}_y$, and correct the image shift, in which the actual time taken is $149ms$. Lastly, fitting x,y,z translation has an average time of $51ms$. From the breakdown, the longest time taken is the image alignment on the frequency amplitude, which typical image alignment on the spatial domain also requires similar timing. Therefore, the whole processing time is reasonable in the current industrial applications.

Conclusions and Future Work

The application of digital holographic microscopy can benefit the semiconductor industry by utilizing extended depth of field for object alignment. This paper proposed a hologram alignment algorithm, which merges the refocusing algorithm with the image alignment algorithm for optimization. The algorithm shows no significant loss in accuracy and robustness among different object patterns through case simulation. Also, the computation time is reasonable to some typical industrial applications.

Further extension on the algorithm's features, such as to handle object imperfections, different pattern types, and image aberrations, could be done. More tests on real images should be carried out to verify the applicability of the algorithm in the field.

References

[1] Dennis Gabor, "A New Microscopic Principle", Nature 161, pg. 777–778 (1948).

[2] Jyoti Mangal, Rashi Monga, Sandeep R Mathur, Amit K Dinda, Joby Joseph, Sarita Ahlawat, and Kedar Khare, "Unsupervised Organization of Cervical Cells Using Bright-field and Single-shot Digital Holographic Microscopy", Journal of Biophotonics, 12.8(2019).

[3] Yves Emery, Etienne Cuche, François Marquet, Nicolas Aspert, Pierre Marquet, Jonas Kühn, Mikhail Botkine, Tristan Colomb, Frédéric Montfort, Florian Charrière, Christian Depeursinge, Patrick Debergh, and Ramiro Conde, "Digital Holographic Microscopy (DHM) for Metrology and Dynamic Characterization of MEMS and MOEMS", Proceedings of the SPIE, 6186.1 (2006)

[4] Emmett N Leith and Juris Upatnieks, "Reconstructed Wavefronts and Communication Theory", Journal of the Optical Society of America, 52.10 (1962).

[5] Joseph W. Goodman, "Introduction to Fourier optics", W.H. Freeman, New York, 2017, pg. 55.

[6] Taegeun Kim, Ting-Chung Poon, and Guy Indebetouw, "Depth Detection and Image Recovery in Remote Sensing by Optical Scanning Holography", Optical Engineering, 41.6 (2002).

[7] Mozhdeh Seifi, Loic Denis, and Corinne Fournier, "Fast Diffraction-pattern Matching for Object Detection and Recognition in Digi-

tal Holograms", 21st European Signal Processing Conference (EUSIPCO 2013), pg. 1-5(2013).

[8] Ujitha Abeywickrema, Rudra Gnawali, and Partha P. Banerjee, "Identification of 3D objects using correlation of holograms", Proceedings of the SPIE 10752, pg. 1075219 (2018).

[9] Georgios D. Evangelidis and Emmanouil Z. Psarakis, "Parametric Image Alignment Using Enhanced Correlation Coefficient Maximization", IEEE Transactions on Pattern Analysis and Machine Intelligence, 30, 10(2008).

[10] Xiaohua Tong, Yusheng Xu, Zhen Ye, Shijie Liu, Lingyun Li, Huan Xie, Fengxiang Wang, Sa Gao, and Uwe Stilla, "An Improved Phase Correlation Method Based on 2-D Plane Fitting and the Maximum Kernel Density Estimator", IEEE Geoscience and Remote Sensing Letters, 12, 9(2015).

[11] Paul W. Holland and Roy E. Welsch. "Robust Regression Using Iteratively Reweighted Least-Squares", Communications in Statistics: Theory and Methods, A6, pg. 813–827(1977).

Author Biography

Fan Hei Hung received the B.S. degree from the University of New South Wales in 2017 . He is currently an MPhil Student at the University of Hong Kong in the Department of Electrical and Electronic Engineering. His research interests include digital holography algorithms and applications.

JOIN US AT THE NEXT EI!

IS&T International Symposium on

Electronic Imaging

SCIENCE AND TECHNOLOGY

Imaging across applications . . . Where industry and academia meet!

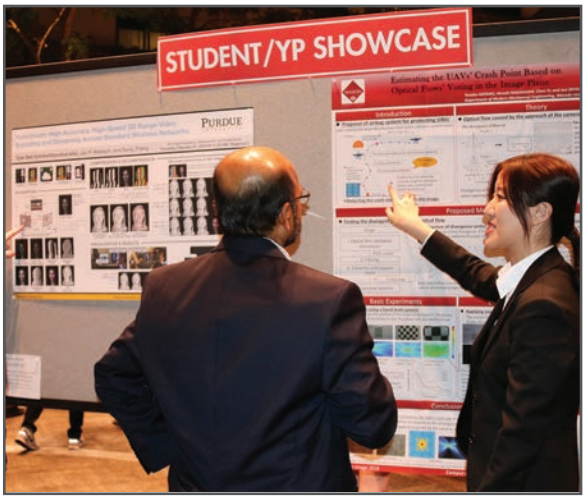

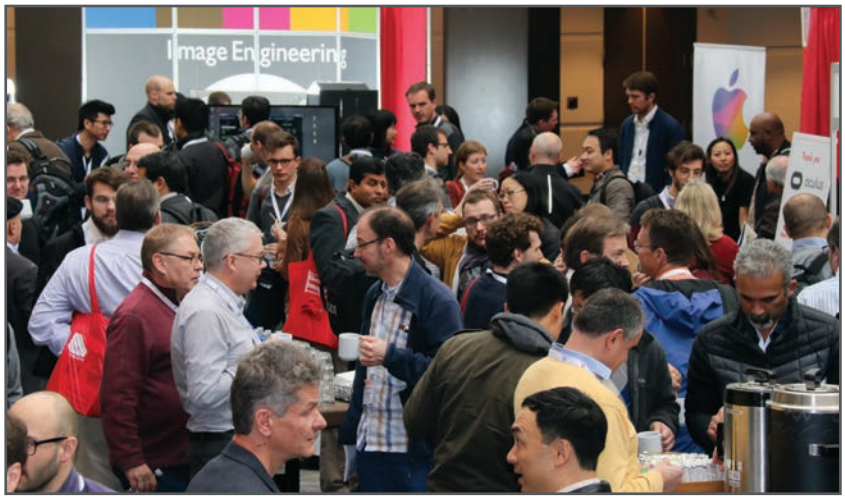

• SHORT COURSES • EXHIBITS • DEMONSTRATION SESSION • PLENARY TALKS •
• INTERACTIVE PAPER SESSION • SPECIAL EVENTS • TECHNICAL SESSIONS •

www.electronicimaging.org

IS&T
imaging.org